Theory of defect states in glassy selenium

David Vanderbilt and J. D. Joannopoulos
Department of Physics, Center for Materials Science and Engineering, Massachusetts Institute of Technology, Cambridge, Massachusetts 02139
(Received 25 February 1980)

A realistic approach to the electronic theory of bond-coordination defects in chalcogenides, based on self-consistent pseudopotential calculations, is used to study glassy Se. The results of the pseudopotential calculations are interpreted in terms of simpler tight-binding models. The onefold and threefold coordination defects are both found to give rise to nondegenerate, nonhydrogenic gap states, whose properties are unique to the chalcogenides in several respects. The existence of π interactions between nonbonding orbitals at defect sites is found to be crucial to an understanding of the electronic structure. These interactions are responsible for large charge transfers between atoms and consequently large energy shifts of atomic valence orbitals, which make these defects quite unlike those in other semiconductors. The origin, character, energy location, and localization of the defect states associated with bond-coordination defects, and with defect pairs and certain relaxed defects, are discussed.

I. INTRODUCTION

In recent years a variety of unusual experimental phenomena in chalcogenide glasses[1-6] have been attributed to the presence of structural defects such as under- or overcoordinated sites.[4-6] This approach had its origins in the suggestion of Anderson that a negative effective correlation energy U, deriving from strong electron-phonon coupling, could explain many of these experiments.[7] Street and Mott then proposed that the negative U is caused by lattice distortions at dangling-bond sites,[4,8] and subsequently Kastner, Adler, and Fritzsche extended this idea by focusing attention on pairs of threefold and singly coordinated chalcogens (valence alternation pairs or VAP's) as the active negative-U centers.[9]

While the defect model is used today to interpret much of the experimental work on chalcogenide glasses, it is not universally accepted.[10-12] Some alternative models[10,11] propose a smooth distribution of bond strengths so that the coordination number of a weakly bonded atom may not be well defined. In these models, the gap may be explained as being due entirely to two-electron effects associated with the negative U; the one-electron gap is completely washed out by large numbers of weak bonds. The defect model, on the other hand, assumes that the intermediate cases (weak bonds) are *less* likely than the extreme cases (broken or extraordinary bonds, i.e., coordination defects). This perspective follows from an implicit principle of chemistry that covalently bonded atoms always seek one of a few natural bonding configurations. Furthermore, it provides a direct identification between the gaps in the amorphous and crystalline phases. We shall adopt the viewpoint of the defect model here. For definiteness, however, we define a bond to be broken when the bond length corresponding to the deep minimum in the radial distribution function is exceeded, which occurs at 3.0 Å in glassy Se.[13]

The existence of the negative U appears to be unique to the chalcogenide glasses.[4] Pnictides and tetrahedrally coordinated amorphous semiconductors apparently do not have the steric freedom to allow sufficient lattice relaxation and cannot easily form extraordinary bonds because of the unavailability of nonbonding orbitals.[5] In addition, it has recently become clear from theoretical work that bond-coordination defects in chalcogenides are unique in several other respects.[14] For example, we will show below that anomalous π interactions with nonbonding orbitals on sites neighboring the defect play an interesting and crucial role in the electronic structure of the defects. Moreover, we show that this and other factors conspire to give the neutral dangling-bond (onefold) defect in selenium an extraordinarily low energy of formation.

The excitement surrounding the unique properties of defects in chalcogenides has motivated us to undertake an in-depth theoretical study. To obtain a satisfactory understanding of the basic physics underlying the structure, ground-state properties, and elementary excitations of these defects, it is necessary to develop a theoretical description which is realistic. Owing to the inherent nonperiodicity of the defect problem, this has been an elusive goal. We have approached the problem by employing a powerful combination of realistic self-consistent pseudopotential (SCPSP) calculations on periodic "superlattice" structures containing defects and by employing flexible tight-binding (TB) techniques which can be used to solve nonperiodic single-defect structures. As a consequence, a theoretical description with several novel and unexpected aspects is

now emerging. In this paper we present this theoretical description in some detail and review the calculations on which it is based. We shall restrict our attention to a-Se as a model system. (In a later paper we will discuss the analogous defects in glassy As_2Se_3, emphasizing similarities and important differences.)

In this paper we consider three kinds of theoretical calculations. The SCPSP calculations employ a realistic Hamiltonian and are self-consistent, but the structure, being periodic, is approximate. Defect states get broadened into bands, and therefore these results do not lend themselves to direct interpretation. However, the SCPSP results were then used as the basis for the fitting of a TB Hamiltonian, which was then applied to more realistic nonperiodic single-defect structures. These "realistic tight-binding" calculations reproduced all of the essential features of the SCPSP results. Moreover, they provided a good physical description of the nature of the defect states. Finally, in order to understand how these defect states arose, we carried out extremely simplified TB calculations on the single-defect structures. While many of the features of the realistic calculations were lost, this exercise was nonetheless very useful in developing a physical intuition about the problem.

Since the purpose of this paper is to present the theoretical understanding which has emerged from this work, the discussion of the SCPSP results and the fitting of the realistic TB Hamiltonian to these results is deferred to Appendix A. In Sec. II we discuss the nature of the electronic states at unrelaxed onefold and threefold defects. We begin with the extremely simplified but intuitively accessible TB model and then discuss in some detail the new physics which arises in the realistic TB calculation. In Sec. III we extend the work to include more complicated defect structures, including close defect pairs and certain kinds of relaxations. In both Secs. II and III we refer to an empirical method for estimating defect total energies which is described in detail in Appendix B. The method used to obtain the density of states for these defect structures is generalized to the case of nonorthogonal basis orbitals in Appendix C. Finally, in Sec. IV we summarize and discuss the implications of the work.

II. ONEFOLD AND THREEFOLD DEFECTS

Our model for the glass will consist of defects embedded in an otherwise perfectly coordinated continuous random network which will be referred to as the "bulk." For the case of glassy Se, this consists of infinite chains (and perhaps some eightfold and larger rings) packed in such a way that bond angles and bond lengths remain approximately those of the crystalline structure. The first step, clearly, is to model the electronic density of states of the bulk. Because the interchain bonding is weak, having considerable van der Waals character, and because the gross features of the density of states are expected to be determined by the short-range order (i.e., the local bonding configuration), we model the bulk random network by focusing on a single "average" chain embedded in the glass. Similarly, an N-fold coordination defect is modeled by attaching N such bulk chains to the defect site. For definiteness we choose a chain identical to that in the trigonal crystal, keeping in mind that bond-angle fluctuations and dihedral-angle disorder may broaden the resulting density of states slightly and introduce narrow band tails. Thus, within a first-neighbor tight-binding point of view, our model for the electronic structure of the bulk has reverted to that of trigonal Se, although the results must be interpreted with the philosophy outlined above in mind.

The electronic structure of these trigonal chains is by now well understood.[15,16] In the valence region, one finds a $4s$-like band fairly well separated from three $4p$-like bands. The latter consist of filled-valence and lone-pair bands and an empty antibonding conduction band.

The origin of the distinct p bands may be understood by referring to Fig. 1(a). Here we have taken an extremely simplified model for trigonal Se which nevertheless contains much of the essential physics. The helical chain is chosen to have bond angles and dihedral angles of exactly 90°, and we use a simple nearest-neighbor tight-binding model with just the three valence p orbitals on each site. Because of the geometry, there are no interactions between the systems of p_x, p_y, and p_z orbitals, so that the three subsystems become decoupled and degenerate. It thus suffices to consider only the system of y orbitals shown explicitly in Fig. 1(a). The only free parameters in the mod-

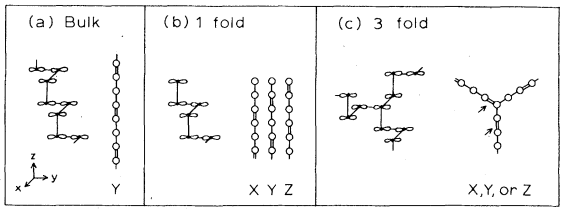

FIG. 1. Structure and interaction diagram (double line V_σ, single line V_π) for (a) helical chain, (b) onefold defect, and (c) threefold defect.

el are a σ-bonding interaction integral V_σ and a weaker π interaction V_π. If we represent these schematically by double and single lines, respectively, we obtain the interaction diagram shown at right in Fig. 1(a).

The origin of the three p bands now becomes clear. In the limit $V_\pi \to 0$, the σ-bonded pairs of orbitals decouple from the remaining nonbonding orbitals (NBO's or "lone pairs"). The latter give rise to a discrete lone-pair level at the unperturbed p energy, while the former produce bonding and antibonding (σ and σ^*) levels below and above the lone-pair level, respectively. For $V_\pi \neq 0$ these three discrete levels must broaden into bands; the resulting density of states is easily calculated and is shown in Fig. 2(a). The σ and lone-pair bands are filled, while the σ^* band is empty. Note that the widths of the bands are determined not simply by a direct π interaction, but rather by a weaker effective interaction of order V_π^2/V_σ, because of the alternation of bond orbitals and NBO's (separated by energy V_σ). This fact will be crucial to the understanding of bond-coordination defects.

Let us consider the simplest such defect, a onefold coordinated (dangling-bond) site terminating a chain in the bulk. This is shown in Fig. 1(b) along with the appropriate interaction diagrams for the systems of x, y, and z orbitals. Note that the three subsystems are still decoupled but no longer identical; each is terminated in a different fashion. The p_z system ends on σ and σ^* orbitals which contribute featurelessly to the bonding and antibonding bands. Similarly, the terminal nonbonding y orbital contributes to the lone-pair band. Of special interest is the system of x orbitals which terminates on a pair of NBO's connected by a direct π interaction. Recall that this is a *stronger* interaction than the effective interaction which determines the lone-pair bandwidth. As a result the two NBO's are split into π bonding and π antibonding combinations [henceforth π(NBO) and π^*(NBO), respectively], giving rise to localized states above and below the lone-pair band edges. This is shown in Fig. 2(b), where the model of Fig. 1(b) is solved exactly using Green's-function techniques. If the defect is neutral, the π^*(NBO) state above the valence-band maximum is half filled (i.e., contains a hole). This defect state will be localized strongly to at most two sites. At this point the existence of localized states at the onefold defect is a consequence of the unique direct π interaction between NBO's on neighboring sites.

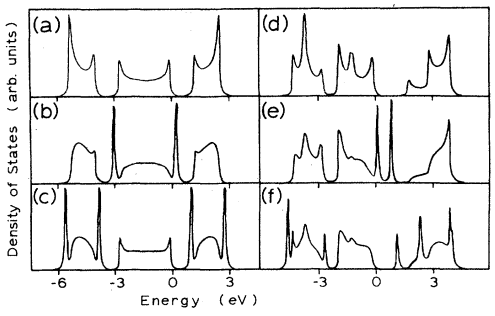

FIG. 2. Local density of states averaged over sites near defect. Using simple TB Hamiltonian: (a) bulk, (b) onefold defect, and (c) threefold defect. Using realistic TB Hamiltonian: (d) bulk, (e) onefold defect, and (f) threefold defect.

Consider now the threefold defect shown in Fig. 1(c). The geometry has been chosen such that there is an exact symmetry of 120° rotation about an axis passing through the threefold site. The decoupled systems of x, y, and z orbitals are once again identical, restoring the threefold degeneracy. We observe a behavior analogous to that at the onefold site. This time there is a pair of σ^* orbitals (and a pair of σ orbitals) shown by arrows which are connected by a direct π interaction. Once again the splitting exceeds the band width, and we expect a pair of threefold-degenerate localized states [$\pi^*(\sigma^*)$ and $\pi(\sigma^*)$ in our notation] to emerge from the antibonding band edges, and similarly for the bonding band. Figure 2(c) shows that this is indeed the case. The threefold degenerate $\pi(\sigma^*)$ state below the conduction-band minimum contains a single electron if the defect is neutral. Note that this state will be highly delocalized, sharing its character among at least the seven central atoms near the defect.

At this point we have seen that onefold defects will tend to produce highly localized defects at the lone-pair band edges, and that threefold defects will give rise to much more delocalized (but still nonhydrogenic) gap states at the bonding and antibonding band edges. Before carrying the discussion further, it becomes essential to improve drastically upon the simple model presented above. We will extend the above discussion by using a much more realistic tight-binding model, but in doing so a fundamental question emerges: How can we be sure that a tight-binding model which has been fit to the bulk density of states will be valid in the neighborhood of the defect? The only way to answer this question is to appeal to realistic first-principles calculations on defect structures. This has been done in Appendix A, where we have applied self-consistent pseudopotential (SCPSP) calculations to crystalline Se and to periodic superlattice structures containing defects. We fit a tight-binding Hamiltonian to the bulk crystal and then determine what modifications to the TB model are necessary to give accurate results

for defects. We find that it is only necessary to adjust the diagonal Hamiltonian matrix elements on the defect sites themselves. The onefold atom has its self-energy shifted upward by 1.25 eV, while the threefold atom is shifted downward by the same amount.

The SCPSP calculations are used to verify the existence of these self-energy shifts in Appendix A, but they can be understood physically in the following way. Suppose we break a single bond in an infinte Se chain, producing two onefold defects. The two electrons which were shared in the σ-bonding orbital each singly occupy a new NBO on the onefold sites. In a simple picture of atomic orbitals, one would then have a hole localized completely on one of the two NBO's on the defect site, and each atom would be individually charge neutral. However, we have shown above that one of the NBO's at the defect interacts strongly with an NBO on the neighboring site, so that in fact the hole is shared between the two sites contributing to the π^*(NBO) defect state. This would lead to a charge of $\pm 0.5\ e$ on the second-to-last and last atoms, respectively. Now the Coulomb interaction shifts the self-energies upward on the terminal atom (and downward on the penultimate one), causing the π(NBO) state to reside mostly on the neighboring site and the π^*(NBO) state to reside mostly on the defect site. The charge transfers and self-energy shifts now adjust themselves self-consistently. When a realistic calculation is done [including, for example, the fact that the π^*(NBO) defect state decays into the bulk], the net result is that the charge transfers are small and the self-energy shift is large only on the defect site itself (see Appendix A).

The situation for the threefold defect is again analogous. The defect atom shares three of its electrons in σ bonds; if the fourth electron could be localized to the defect site, each atom would be individually neutral. Instead, the electron is shared in the highly delocalized $\pi(\sigma^*)$ defect state. The self-consistent process leads to a lowered self-energy on the threefold atom which strongly reduces the amount of charge transfer from the defect site.

When these self-energy shifts are included, we obtain the realistic tight-binding Hamiltonian presented in Table I. The TB model includes s as well as p states with s-p interactions, overlaps between orbitals on neighboring sites, and self-energy shifts of ± 1.25 eV on onefold and threefold sites, respectively. The defect structures to be considered are identical to those of Fig. 1 except for the distortion necessary to obtain the experimental bond angle of 102.54° and the dihedral angle of 100.27°.[17,18]

TABLE I. Tight-binding Hamiltonian for selenium. E is diagonal matrix element, V is nearest-neighbor interaction, and S is nearest-neighbor overlap. Δ_m is change in E_s and E_p at m-fold defect site.

E_s	E_p	Δ_1	Δ_3
−13.00 eV	−1.10 eV	+1.25 eV	−1.25 eV
V_{ss}	V_{sp}	$V_{pp\sigma}$	$V_{pp\pi}$
−2.27 eV	−2.07 eV	−2.97 eV	−1.19 eV
S_{ss}	S_{sp}	$S_{pp\sigma}$	$S_{pp\pi}$
0.08	0.08	0.13	0.15

These structures have been solved within the TB Hamiltonian. The introduction of overlaps introduces subtleties which are discussed in Appendix C. The results are shown for the bulk chain, onefold defect, and threefold defect in Figs. 2(d), 2(e), and 2(f), respectively. The effect of the self-energy shift can be seen dramatically in Fig. 2(e). The π(NBO) and π^*(NBO) states both have substantial character on the defect site and so are strongly influenced. The former moves up in energy and becomes a resonance just above the lone-pair-band minimum, while the latter moves deep into the gap, forming a state near midgap. This state is highly localized to the defect atom, having 68% of its character there and 21% on the neighboring site. Remarkably, there is a second state emerging into the gap just above the valence-band maximum. This corresponds to the terminal nonbonding y orbital of Fig. 1(b) which is also severely influenced by the self-energy shift.

Consider now the threefold site, Fig. 2(f). Recall that the simple model of Fig. 2(c) gave rise to threefold-degenerate defect states above and below both the bonding and antibonding bands. Now taking the bond angles and dihedral angles different from 90° breaks the threefold degeneracy of these states. The $\pi(\sigma^*)$ state in the fundamental gap, for example, splits into a nondegenerate (A-like) state deeper in the gap and a twofold-degenerate (E-like) resonance above the conduction-band minimum. The self-energy shift tends to move these states further downward in energy, but the effect is not dramatic because no state is primarily localized to the defect atom. The defect state occurs 0.55 eV below the conduction-band edge and is highly delocalized, having no more than about 15% of its character on any one site.

In order to appreciate the uniqueness of these defects in chalcogenides, consider for a moment the corresponding defects in pnictide or tetrahedral semiconductors, e.g., a-As or a-Si. First of all, overcoordinated sites are not expected at all in Si. If they exist in a-As, their properties would

be determined by the exceptional sp_3 hybridization at the defect site. Pollard and Joannopoulos[19] have shown that the central σ^* bond orbitals, composed of sp_3 and p orbitals on the fourfold and neighboring sites, respectively, are split by the dehybridization interaction into a T_2-like resonance in the conduction band and an A-like gap state near the conduction-band edge. The gap state is essentially localized to the fourfold site and its immediate neighbors and has no p character on the defect site. This state is thus completely different from the overcoordinated a-Se defect state in origin, character, and symmetry. Thus the chalcogenides are the only systems where one finds such an elegant correspondence between the properties of under- and overcoordinated defects.

Secondly, even the undercoordinated defects are unique in the chalcogenides. The situation is sketched in Fig. 3. In a-As or a-Si, one finds neighboring p or sp_3 orbitals split into σ and σ^* bond orbitals, which are then broadened into valence and conduction bands. A dangling bond simply gives rise to a p or sp_3 orbital which is not bonded away by the σ interaction and which, therefore, remains sitting near midgap. Because there are no such nonbonded orbitals on neighboring sites with which to interact, these defect states are initially strongly localized to the defect atom. Thus no self-consistent charge transfers or self-energy shifts are expected. This is in complete contrast to the case of the chalcogenides, where the availability of neighboring NBO's and the unique π interaction give rise to the rich structure described above.

Bishop, Strom, and Taylor[20] have identified the photoinduced electron spin resonance (ESR) center in selenium as a gap state localized primarily to a single nonbonding orbital. This fits in nicely with our picture of the onefold defect and indicates therefore that onefold defects may be preferred

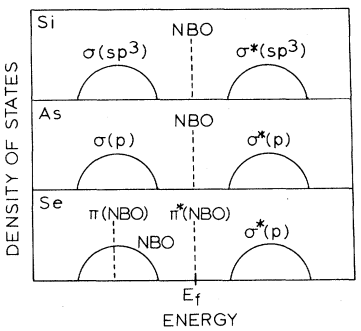

FIG. 3. Sketch of the gap region for undercoordinated defects in group IV, V, and VI semiconductors. The valence and conduction bands are shown schematically. Dashed lines correspond to defect states or resonances.

to threefold defects in the glass. This would be surprising, however, in light of the suggestion by Kastner *et al.* that the lowest-energy neutral defect would be threefold coordinated.[9] This was based on the observation that the threefold defect has an extra bond compared to the onefold, and that consequently the electronic energy of bond formation would favor the threefold. From elementary models based on discrete bond-orbital energy levels, the energies of the onefold and threefold defects were estimated to be ~3–4 eV and ~1 eV, respectively.[5]

However, such an analysis omits the ion-ion repulsion which stabilizes the bonds and fails to take into account the broadening of molecular-orbital levels into bands and the existence of gap states and resonances near defects. The calculated density of states in Fig. 2(e) or 2(f) contains all the information necessary to sum correctly the latter one-electron energies, and the additional repulsive term can be empirically modeled as a constant correction per bond. This is carried out in detail in Appendix B.

The resulting total energies of the onefold and threefold defects are estimated at 1.17 and 1.56 eV, respectively. Three effects are responsible for this remarkable lowering of the energy of the onefold site. Firstly, the ion-ion repulsion largely compensates for the loss of electronic binding energy when a bond is broken. Secondly, the hole which is constrained to lie at the NBO level in the simple models rises from midband to the valence-band edge and beyond in our calculation. Thirdly, the partial π bond between the defect site and its neighbor along the chain stabilizes this defect even further. The net result is that the onefold defect has its energy lowered by about 3 eV. The first and second effects have analogs for the case of the threefold defect which raise and lower the total energy, respectively. The net result is a slight increase of ~0.5 eV in the defect formation energy.

The energy estimates given here apply only to neutral defects. In order to address such questions as the negative U or the luminescence Stokes shift, it will be necessary to identify the lowest-energy charged defects as well. On the one hand, it may be that the defect retains its basic bonding configuration upon change of charge state, with only modest changes in bond lengths and bond angles (bond relaxations). On the other hand, the large Stokes shift would argue that a bond-switching or coordination relaxation can take place. This would be the case, for example, if the lowest-energy positively charged defect were threefold coordinated. An investigation of charged defects is currently underway in order to resolve such ques-

tions.

Because bond relaxations away from the crystalline bond lengths and angles could cause reductions in the neutral-defect energies (on the order of a tenth of an eV), and because of our rough model for ΔU_0, the energies reported above are not final and merely point out the need for more realistic calculations. In particular, lower defect energies are needed if $\sim 10^{17}$ cm^{-3} defects are to be frozen in at the glass transition temperature. We have recently extended the self-consistent pseudopotential calculations to the evaluation of neutral-defect total energies and relaxation energies.[21] We found sufficiently low energies to give $\lesssim 10^{15}$ cm^{-3} coordination defects. However, we wish to emphasize the inadequacy of simple models which are based on bond-orbital levels, or which neglect repulsive interatomic terms, and to point out the plausibility of having the onefold be the favored neutral defect in the glass.

III. COMPLEX DEFECT STRUCTURES

So far, the discussion has been limited to individual onefold and threefold sites, the simplest structural defects. However, once the TB Hamiltonian has been established, it is straightforward to make the extension to more complicated defects and interacting defect pairs. In particular we shall discuss nearest-neighbor onefold and threefold pairs ("intimate valence alternation pairs," or IVAP's),[9] the transition from threefold to onefold coordination, and dihedral-angle variations for the simple defects.

Because onefold and threefold defects are expected to be oppositely charged, the resultant Coulomb attraction will tend to favor close defect pairs.[9] The extreme form of this pairing is the IVAP shown in Fig. 4(c) [together with isolated onefold and threefold defects in Figs. 4(a) and 4(b) for comparison]. Here the onefold and threefold defects are nearest neighbors. The defect states associated with the two defect sites remain, but are shifted closer to the band edges. For the onefold defect, this occurs because the strong direct π interaction, which previously pushed the defect state deep into the gap, disappears due to the absence of an available NBO on the neighboring threefold site. Similarly, the electron trap state becomes more shallow in the IVAP because the strong direct π interaction connects only one pair of σ^* orbitals, rather than three, in the neighborhood of the threefold site.

For an overall neutral IVAP the defect states near the valence-band edge are occupied and the state near the conduction-band edge is empty. Thus, when a pair of isolated neutral onefold and threefold defects are brought together in this fashion, an electron transfer from the threefold to the onefold state occurs. Surprisingly, all sites remain individually almost neutral. This is a remarkable consequence of the self-energy shifts, together with the fact that the defect states are not strictly localized to the defect site.

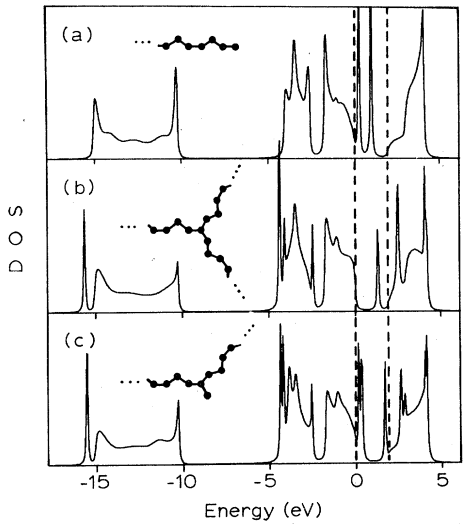

FIG. 4. TB density of states for (a) onefold defect, (b) threefold defect, and (c) IVAP. The structures are shown schematically. Dashed lines represent the gap edges.

From experiments on transport properties during thermal cycling below the glass transition temperature, Abkowitz[22] has found a close correlation between a population of electron traps 0.33 eV below the conduction-band edge and hole traps 0.25 eV above the valence-band edge. In light of our results, these experiments can be plausibly explained by assigning both states to IVAP's, whose density in the glass presumably varies with temperature according to the free energy of defect formation.[9] The method of Appendix B gives a total energy of 1.22 eV for this defect. (Recall that the total energies of the onefold and threefold defects were 1.17 and 1.56 eV, respectively.) This indicates that the IVAP (which is really a defect *pair*) is comparable in energy to an isolated onefold or threefold site and may therefore occur at comparable densities. The energy of 1.22 eV is still too large to allow a sufficient number of defects to be frozen in at the glass transition, but it could be reduced substantially by minimizing with respect to bond relaxations in the defect vicinity. In any case, a quantitative comparison with the results of Abkowitz would require a more realistic calculation than we have performed.

An interesting feature of glassy Se is the possibility of interconversion of onefold and threefold defects. Figure 5 shows the density of states in

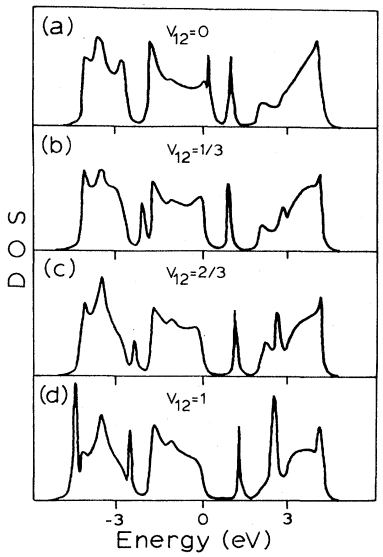

FIG. 5. Change in the density of states as a onefold site bonds to a nearby twofold site. V_{12} is the onefold-twofold interaction in units of the normal nearest-neighbor interaction (a) onefold defect and intact chain, (b) weak interaction, (c) moderate interaction, and (d) threefold defect.

the defect region as a onefold atom swings over and bonds with an atom of a neighboring chain, creating a threefold defect. As one creates the threefold defect, two NBO's interact and contribute a σ and σ^* state. One of these can be clearly seen moving from the lone-pair to the bonding band in Fig. 5. In the fundamental gap, however, the deep defect state simply changes from being an NBO-derived state to being a σ^*-derived state while shifting only very slightly in energy.

Finally, in Fig. 6 we show the energy location of the deep defect level as a function of dihedral-angle variations for isolated onefold and threefold defects. This case has been chosen as a likely example of possible relaxations at the defect site because the constraint on dihedral angle is not expected to be as strong as that on bond length or bond angle. Note that the onefold level is not strongly affected, while the threefold level is quite sensitive. In both cases the eigenvalue has a minimum near the crystalline dihedral angle. For neutral defects these levels are singly occupied, suggesting that the dihedral angle probably does not deviate greatly from the unrelaxed value. This has been verified in the case of the onefold defect.[21]

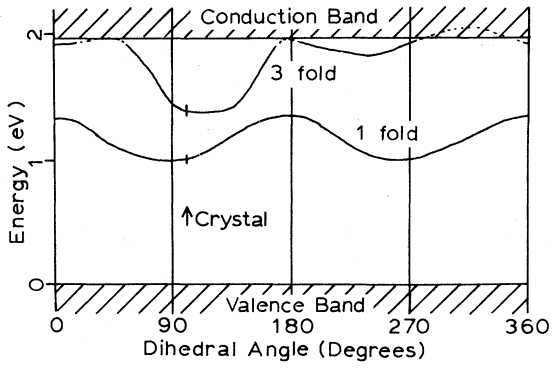

FIG. 6. Energy levels of defect gap states as a function of dihedral angle on (i) the next-to-last bond for the onefold defect and (ii) the three bonds connecting to the defect site for the threefold defect.

IV. SUMMARY AND CONLCUSIONS

We have developed an approach to the study of structural defects in chalcogenides which makes use of flexible tight-binding techniques while remaining grounded in realistic self-consistent pseudopotential calculations. A variety of defect structures are studied. The neutral onefold coordinated defect gives rise to a deep-hole trap state near midgap. This state is highly localized near the defect site, as it derives from a π-antibonding combination of nonbonding orbitals on the defect site and its neighbor along the chain. The neutral threefold defect produces a less localized but nonhydrogenic nondegenerate electron-trap state below the conduction-band edge, which derives from a π-bonding combination of antibonding orbitals. The IVAP gives rise to both of these defect states, but they are closer in energy to the band edges.

The results emphasize the unique nature of defects in chalcogenides as opposed to other amorphous semiconductors. In particular, the availability of nonbonding orbitals on sites neighboring the defect atom allows the formation of an anomalous π bond at the undercoordinated defect and gives rise to the positive self-energy shift. We find a remarkable degree of analogy between the behavior of the onefold and threefold defects. The latter has an anomalous π interaction between antibonding orbitals which gives rise to an electron trap and a negative self-energy shift. This parallelism can occur only in the chalcogenides, where overcoordinated defects can form freely because no s-p hybridization is required. We expect that defects in a-As, a-Si, and even a-As_2Se_3 will be quite different in electronic structure than those in Se.

ACKNOWLEDGMENTS

We wish to extend thanks to Mark Kastner for many valuable discussions, and to Robert Laughlin for suggestions relevant to Appendix C. This work

was supported in part by National Science Foundation Grant No. DMR76-80895. We should also like to acknowledge additional support from the National Science Foundation and the Alfred P. Sloan Foundation.

APPENDIX A: SELF-CONSISTENT PSEUDOPOTENTIAL CALCULATIONS

To provide a realistic foundation for the tight-binding Hamiltonian of Table I, we have carried out self-consistent pseudopotential (SCPSP) calculations on a variety of periodic structures containing bond-coordination defects. In this appendix we describe the structures which have been solved, discuss the method, review the results of these calculations, and present the fitting of the TB Hamiltonian to the SCPSP results.

In Fig. 7 we show trigonal Se and two periodic structures containing defect pairs. The defect structures have unit cells containing six atoms, instead of the usual three, and are made simply by adjusting some of the atomic positions so as to break bonds or form new bonds. The structures are chosen so that all of the bond lengths and bond angles match exactly those of trigonal Se (which we take to be 2.390 and 102.48 Å, respectively).[17,18] In model A, each unit cell contains a onefold defect and a threefold defect as third neighbors along a chain; model B represents the IVAP. We have also solved structures, not shown here, which contain 11 atoms per unit cell such that each cell contains two identical onefold defects (or two identical threefold defects). The latter results merely verify that the coexistence of onefold and threefold defects together in model A has no influence on the important physics (e.g., the existence of self-energy shifts). For our purposes here, it will be sufficient to focus only on a comparison between the results for the trigonal crystal and for model A.

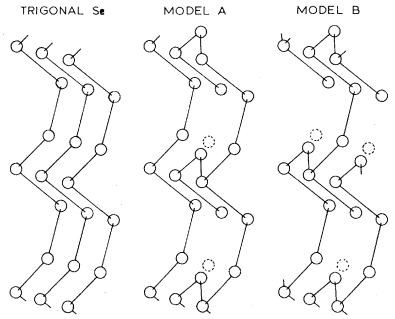

FIG. 7. Periodic structures to which SCPSP can be applied. Dotted circles represent unperturbed lattice positions.

The self-consistent pseudopotential approach has been described in detail elsewhere.[23] The selenium cores are represented by a local ionic pseudopotential which has been chosen once and for all such that when self-consistently screened, the valence levels match the published Herman-Skillman eigenvalues for the atom.[24] (Throughout this appendix, screening is calculated by using Slater $\rho^{1/3}$ exchange, with a coefficient $\alpha = 1$, for the exchange-correlation term.) Once fit to the atom in this way, the pseudopotential is used without modification for all subsequent crystal calculations; in this sense, these are first-principles calculations.

The crystalline pseudopotential is just the sum of the ionic pseudopotential on each atomic site plus the screening from the valence electrons. These electrons are represented using a plane-wave basis. All plane waves with $q < 3.67$ Å^{-1} have been included, and those with $q < 5.93$ Å^{-1} have been included in Lowdin perturbation theory[25] when solving for the wave functions. For trigonal Se, this corresponds to 70 and 300 plane waves, respectively; for model A, 140 and 600. The charge densities are averaged over the Brillouin zone using Chadi's special-points scheme,[26] with 3 and 8 k points in the irreducible Brillouin zone for trigonal Se and model A, respectively.

The density of states for trigonal Se is shown

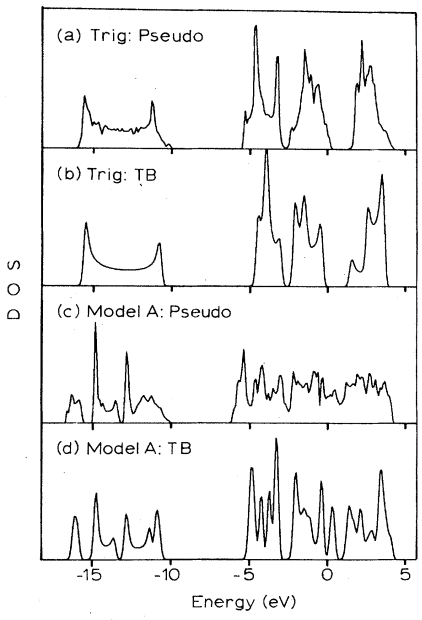

FIG. 8. Theoretical electronic density of states for periodic structures: (a) SCPSP applied to trigonal Se, (b) tight-binding fit for trigonal Se, (c) SCPSP applied to model A, and (d) tight-binding fit for model A.

in Fig. 8(a). One finds filled s,p bonding, p lone-pair bands, and an unfilled p antibonding band. In Fig. 8(b) we show the density of states for the tight-binding Hamiltonian of Table I. The fitting has been done by artificially reducing the SCPSP band structure to a 1-d band structure $E=E_n(k_\parallel)$, by averaging over all $k_\perp$ for each $k_\parallel$ (the orientations are with respect to the chain axis). The TB Hamiltonian was then adjusted to match the band edges of this 1-d band structure as closely as possible. As can be seen from Figs. 8(a) and 8(b), this results in satisfactory agreement between the full SCPSP and TB densities of states.

Figure 8(c) shows the SCPSP density of states for model A. Because of lowered symmetry, the s-like band has broken into three subbands. In the p region, gap states have been broadened into defect bands (by interdefect interactions), and the gaps have thus been obscured. In Fig. 8(d) we show the corresponding TB calculation on the same structure. Now the self-energy shifts in the Hamiltonian of Table I come into play. These were chosen by actually integrating in real space to calculate the diagonal matrix elements of the converged self-consistent potential between atomic (Herman-Skillman)[24] orbitals centered on each atomic site. The calculated self-energy shift on the onefold site was 1.27 eV, on the threefold site −1.24 eV, and the other four sites ranged from −0.38 to 0.28 eV. For simplicity we have ignored the self-energy shifts on twofold coordinated sites and approximated those on the defect sites as ±1.25 eV. A comparison of Figs. 8(c) and 8(d) indicates that this fitting is adequate. Note, in particular, the agreement in the s region; without the self-energy shifts, there was little resemblance here between the SCPSP and TB results.

An approximate measure of the charge on each site in model A was obtained by integrating the SCPSP valence-charge density over a sphere, with radius equal to half the bond length, centered about each atomic site. (Such an estimate is somewhat arbitrary, but should at least reveal any large charge transfers.) Each site was found to be individually neutral to within ±0.06 e. This is surprising because a charge transfer from the threefold to the onefold site would have been expected on the basis of simple chemical arguments. The lack of charge transfer is a result of the compensating effect of the self-energy shifts, which tend to attract electrons to the threefold site and repel them from the onefold site. Thus, the SCPSP calculations on model A can be considered to refer to neutral defects. The SCPSP method has been extended to allow the calculation of total energies for structures containing defects; this work will be reported in a later paper.[21]

APPENDIX B: EMPIRICAL TOTAL-ENERGY CALCULATIONS

Once we have obtained the density of states in the vicinity of the defect from the realistic tight-binding calculation, it is relatively straightforward to find the band-structure energy $E_{\rm BS}$ which is just the sum of filled one-electron levels. However, the total energy is not simply $E_{\rm BS}$, but contains the repulsive Coulomb interactions between ion cores and other corrections.

In order to write down the total energy, we adopt the Hartree-Fock-Slater point of view and consider the system to be composed of valence electrons and frozen ion cores of charge $Z=+6$ for Se. Then the total energy is [27]

$$E_T=\sum_i \int d\vec{r}\,\psi_i^*(\vec{r})\left(-\frac{h^2}{2m}\nabla^2+V_{\rm ion}(\vec{r})\right)\psi_i(\vec{r}) + \tfrac{1}{2}\sum_i \int d\vec{r}\,V_H(\vec{r})\,|\psi_i(\vec{r})|^2 + \tfrac{3}{4}\sum_i \int d\vec{r}\,V_{x\alpha}(\vec{r})\,|\psi_i(\vec{r})|^2 + \tfrac{1}{2}\sum_{nm}\frac{e^2Z^2}{|\vec{R}_n-\vec{R}_m|}=E_{\rm BS}+U\,, \tag{B1}$$

where V_H and $V_{x\alpha}$ are the Hartree and Slater exchange potentials. The corrections to $E_{\rm BS}$ have been lumped together in the term U. Since

$$E_{\rm BS}=\sum_i \epsilon_i=\sum_i \int d\vec{r}\,\psi_i^*(\vec{r})\left(-\frac{h^2}{2m}\nabla^2+V_{\rm ion}(\vec{r}) + V_H(\vec{r})+V_{x\alpha}(\vec{r})\right)\psi_i(\vec{r})\,, \tag{B2}$$

we can write

$$U=\sum_i \int d\vec{r}\,[-\tfrac{1}{2}V_H(\vec{r})-\tfrac{1}{4}V_x(\vec{r})]\,|\psi_i(\vec{r})|^2 + \tfrac{1}{2}\sum_{nm}\frac{e^2Z^2}{|\vec{R}_n-\vec{R}_m|}\,. \tag{B3}$$

The term U thus contains corrections due to overcounting of the Hartree and exchange-correlation energies [the Coulomb repulsion between each pair of electrons was counted twice in Eq. (B2)] and the repulsive ion-ion interaction. There is little hope of evaluating this term directly within the tight-binding model, so we turn instead to a rough empirical approach.

In Fig. 9 we sketch the dependence of E_T, $E_{\rm BS}$, and U as a function of bond length for a uniform expansion or contraction of the trigonal crystal. Here we have taken the atom as the zero of energy. This corresponds to taking the bond length $d\to\infty$. The cohesive energy of the crystal E_b is given by

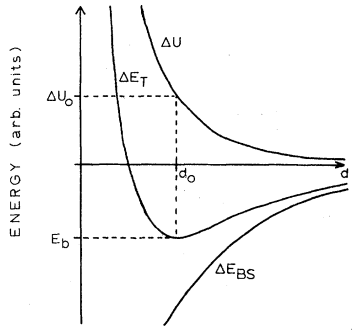

FIG. 9. Sketch of contributions ΔE_{BS} and ΔU to the total energy per bond ΔE_T, as a function of bond length d.

the minimum of E_T which occurs at the equilibrium bond length d_0. We can expand ΔU as a function of d about d_0 (Ref. 28):

$$\Delta U = \Delta U_0 + \alpha(d-d_0) + \tfrac{1}{2}\beta(d-d_0)^2 + \text{higher terms}. \quad \text{(B4)}$$

Since ΔE_{BS} can be calculated as a function of d, it is possible to obtain the constants ΔU_0, α, and β if the binding energy and bulk modulus are known experimentally.

Since it is very difficult to calculate U for an arbitrary structural configuration, it is necessary to introduce a simplifying assumption at this point. Following Chadi[28] we assume

$$U = \sum_l \Delta U(d_l), \quad \text{(B5)}$$

where l labels first-neighbor covalent bonds in the material and d_l is the corresponding bond length. This approach has been used previously to estimate the relaxed bond length at semiconductor surfaces[28] where only α and β need be known. In the present context, however, we assume bonds are either normal ($d=d_0$) or completely broken. Thus we need only find a way to estimate the equilibrium value ΔU_0. Having done so, we calculate the total energy of any defect structure by integrating over the density of states to obtain E_{BS} and correcting by $\mp\Delta U_0$ for each broken or extra bond in the structure. (From now on, E_T and B_{BS} will always be referred to the energy of an equal number of atoms in the normally coordinated bulk as the zero of energy.) We will describe the calculation of E_{BS} in detail shortly, but let us first estimate ΔU_0.

The most straightforward way to determine a value for ΔU_0 would be to imagine the dissociation of trigonal Se into separate atoms. Then E_T is the experimental cohesive energy per atom E_b = 2.35 eV,[29] and $U = E_T - E_{BS} = -\Delta U_0$. The determination of E_{BS} is complicated, however, by the fact that in our Hamiltonian, the atomic-orbital energy levels on each atom are shifted as a function of the coordination of that atom. The self-energy shifts for threefold, twofold, and onefold sites are $\Delta_3 = -1.25$ eV, $\Delta_2 = 0$ eV, and $\Delta_1 = 1.25$ eV. If there were no self-energy shift on the free atom, we would find $E_{BS} = 4.47$ eV. A simple extrapolation gives $\Delta_0 = 2.50$ eV, $E_{BS} = 19.47$ eV, and $\Delta U_0 = 17.12$ eV. However, we have little confidence in such an extrapolation, and we prefer instead to find an experimental reference which does not involve free atoms.

This has been accomplished by considering the dissociation of the trigonal crystal into free Se_2 molecules instead of free atoms. To be precise, we proceed conceptually in the following stages: (i) dissociate the crystal into free atoms; (ii) combine free atoms to form Se_2 dimers; and (iii) adjust the bond length of the dimer to be d_0. The corresponding energy gains of the system, per two atoms at 0 K, are (i) $2E_b = 4.70$ eV (Ref. 29); (ii) -72.96 kcal/mole $= -3.18$ eV (Ref. 30); and (iii) 0.46 eV from vibrational data.[31] Thus for the entire process $E_T = 1.98$ eV. The calculation of the corresponding E_{BS} is straightforward. Applying the Hamiltonian of Table I to the dimer, we calculate $E_{BS} = 17.83$ eV and, therefore, $U = E_T - E_{BS} = -15.85$ eV. Since this corresponds to breaking one bond, we have finally $\Delta U_0 = 15.85$ eV. It is this value we will use for all subsequent calculations of defect total energies.

Our goal now is to determine E_{BS} and U for the onefold defect, threefold defect, and IVAP of Fig. 4. Because two onefold (threefold) defects are required to break (form) a single bond, we have $U = \mp\frac{1}{2}\Delta U_0$ and 0 for these three cases, respectively. We turn now to a detailed discussion of the evaluation of E_{BS}.

Recall that E_{BS} is now defined with respect to an equal number of atoms in the normally coordinated bulk, as a zero of energy. Thus if $N_n(\epsilon)$ is the local density of states on the nth site and $N^0(\epsilon)$ is the local density of states at any site in the bulk, we can write

$$E_{BS} = \sum_n \int_{-\infty}^{\epsilon_F} \epsilon\,\delta N_n(\epsilon)\,d\epsilon, \quad \text{(B6)}$$

where ϵ_F is the Fermi level and $\delta N_n(\epsilon) = N_n(\epsilon) - N^0(\epsilon)$. The energy integral is carried out numerically, and the sum over sites is typically well converged (within ~0.01 eV) with the inclusion of the first 10 sites extending down each of the semi-infinite chains attached to the defect.

There is one fine point which arises in the evaluation of the energy integral. In the Green's-function formalism, the density of states is

$$N_n(\epsilon) = -\frac{1}{\pi}\,\mathrm{Im}\sum_\alpha \frac{|\langle n|\alpha\rangle|^2}{\epsilon - \epsilon_\alpha + i\delta}, \tag{B7}$$

where α are eigenstates of the system and δ is a small imaginary part which must be included in the calculation. Thus each eigenstate contributes to the total density of states as

$$\frac{1}{\pi}\frac{\delta}{(\epsilon-\epsilon_\alpha)^2+\delta^2}.$$

This is a Lorentzian which goes to a delta function in the limit $\delta \to 0$. For calculational purposes, δ is chosen to be comparable to the energy mesh spacing and is typically 0.04 eV. The fact that a nonzero δ must be employed in the calculation has two unfortunate consequences. Firstly, the density of states does not quite drop to zero in the gap regions (see, for example, Figs. 3–5), so that it can be hard to decide where to put the Fermi level in the gap. Secondly, and more seriously, the energy integral over the tail of the Lorentzian goes as

$$\int_{-\infty}^{-x} \epsilon \frac{1}{\pi}\frac{\delta}{(\epsilon-\epsilon_\alpha)^2+\delta^2}d\epsilon \cong \frac{\delta}{\pi}\int_{-\infty}^{-x}\frac{d\epsilon}{\epsilon},$$

and is therefore logarithmically divergent.

We have corrected these problems by deconvoluting the Lorentzian out of the density of states, and subsequently broadening by a Gaussian of the same width. Using standard fast-Fourier-transform routines, we numerically transform the density of states, divide and multiply by the transforms of the Lorentzian and Gaussian, respectively, and then reverse transform back to energy space. Because the Gaussian falls off much faster in the tail regions, the divergences disappear and the density of states in the gap typically falls to a value several orders of magnitude lower than it did previously. This appears to be a simple yet general technique for obtaining an accurate energy integral.

The above program has been carried out to calculate the total energies of the onefold, threefold, and IVAP defects of Fig. 4. The results are shown in Table II. The last three columns represent total energy estimates of increasing sophistication.

TABLE II. Total-energy calculation for defects. First two columns are contributions to E'_{BS} or E_T; last three are total energy estimates of increasing sophistication. See text.

	E_{BS} (eV)	U (eV)	E_{SBO} (eV)	E'_{BS} (eV)	E_T (eV)
onefold	9.09	−7.92	3 − 4	1.59	1.17
threefold	−6.36	7.92	1	1.14	1.56
IVAP	1.22	0.0	?	1.22	1.22

E_{SBO} refers to "simple-bond-orbital" estimates[9] which are based on discrete bond-orbital electron levels and which neglect inter-ion repulsion entirely. The quantity $E'_{BS} = E_{BS} - Z\Delta_{1\text{ or }3}$ is essentially our calculated E_T, except that only that portion of U necessary to cancel the strong effects of the self-energy shifts in E_{BS} is included. Thus E_T effectively includes the ion-ion repulsion, while E'_{BS} does not. Note the striking reversal in the relative onefold and threefold energies in the last three columns. The physical significance of these results is discussed in Secs. II and III of the text.

APPENDIX C: SOLUTION OF THE CLUSTER-BETHE-LATTICE WITH NONORTHOGONAL-BASIS ORBITALS

The solution of the Hamiltonian of Secs. II and III, for a structure composed of a defect with semi-infinite chains attached to represent the bulk, is solved in the spirit of the cluster-Bethe-lattice method (CBLM)[32,33] using Green's-function techniques. The method of the present calculation is in fact identical to the CBLM for a system of twofold coordination, except that the solution has been generalized to allow nonorthogonal-basis orbitals. To our knowledge, such a generalization has not been previously reported. Because there are many systems for which the inclusion of nearest-neighbor overlaps is natural and useful, we outline the method in this appendix. The discussion will specialize to systems of twofold coordination, but the generalization to higher coordination is straightforward.

We begin by defining the Green's-function operator

$$\mathcal{G}(E) = (E - \mathcal{H})^{-1} = \sum_\alpha \frac{|\psi_\alpha\rangle\langle\psi_\alpha|}{E - E_\alpha}. \tag{C1}$$

$\mathcal{H}$ is the Hamiltonian, the $|\psi_\alpha\rangle$ are energy eigenstates with eigenvalues E_α, and the energy $E = \epsilon + i\delta$ is taken to have an infinitesimal imaginary part. Then

$$-\frac{1}{\pi}\,\mathrm{Im}\,\mathrm{tr}\mathcal{G} = \sum_\alpha \delta(\epsilon - E_\alpha) = n(\epsilon) \tag{C2}$$

gives the density of states. Now choose basis vectors $|i\rangle$, linearly independent but not necessarily orthonormal, and construct the duals $|i^*\rangle$ such that

$$\langle i^*|j\rangle = \delta_{ij}, \tag{C3}$$

and therefore

$$\sum_i |i^*\rangle\langle i| = 1. \tag{C4}$$

Define the generalized Green's-function matrix elements as

$$G_{ij} = \langle i^* | \mathcal{G} | j \rangle . \tag{C5}$$

Using Eqs. (C1) and (C4), one easily shows

$$-(1/\pi)\mathrm{Im}\,\mathrm{tr}G = n(\epsilon) , \tag{C6}$$

so that the natural definition of the local density of states is

$$-(1/\pi)\mathrm{Im}G_{ii} = n_i(\epsilon) . \tag{C7}$$

Taking matrix elements, Eq. (C1) can be recast into the form

$$\sum_j \langle i | E - \mathcal{H} | j \rangle \langle j^* | \mathcal{G} | k^* \rangle = \delta_{ik} . \tag{C8}$$

We define

$$\begin{aligned} S_{ij} &= \langle i | j \rangle , \\ H_{ij} &= \langle i | \mathcal{H} | j \rangle , \\ \tilde{G}_{ij} &= \langle i^* | \mathcal{G} | j^* \rangle , \end{aligned} \tag{C9}$$

where the basis is assumed to have been chosen such that the S_{ij} and H_{ij} are real. Equation (C8) now becomes

$$\sum_j (ES_{ij} - H_{ij})\tilde{G}_{jk} = \delta_{ik} . \tag{C10}$$

G is related to $\tilde{G}$ by

$$G_{ij} = \sum_k \tilde{G}_{ik} S_{kj} . \tag{C11}$$

We will proceed by solving first for $\tilde{G}$, then G.

In typical applications we label orbitals by a site label "i" and an internal label "a" which runs over the N atomic orbitals on each site. In this notation, each matrix element (H_{ij}, S_{ij}, etc.) is itself an $N \times N$ matrix in the internal space. We adopt this convention and furthermore restrict ourselves to first-neighbor interactions and overlaps for the purpose of this discussion. Thus for bulk Se, which corresponds to a 1-d chain of sites, the inputs are the matrices

$$\begin{aligned} S_0 &\equiv S_{ii} , \\ S &\equiv S_{i,i+1} , \\ E_0 &\equiv ES_{ii} - H_{ii} , \\ V &\equiv H_{i,i+1} - ES_{i,i+1} . \end{aligned} \tag{C12}$$

Note that S_0 and E_0 are symmetric and that $S_{i+1,i} = S^T$, etc.

When attached to a defect, the chain segment under consideration will extend uniformly to infinity in one direction ($i \to +\infty$) and will be attached to a defect at $i = 0$. If we define the fields χ_i and $\bar{\chi}_i$ by

$$\begin{aligned} \tilde{G}_{i+1,\,i-n} &\equiv \chi_i V^T \tilde{G}_{i,\,i-n} \\ \tilde{G}_{i-1,\,i+n} &\equiv \bar{\chi}_i V \tilde{G}_{i,\,i+n} \end{aligned} \tag{C13}$$

for $n > 0$, Eq. (C10) gives, e.g.,

$$\begin{aligned} &E_0\tilde{G}_{i,\,i-n} - V\tilde{G}_{i+1,\,i-n} - V^T\tilde{G}_{i-1,\,i-n} = 0 , \\ &(E_0\chi_{i-1} - V\chi_i V^T\chi_{i-1} - 1)V^T\tilde{G}_{i-1,\,i-n} = 0 , \end{aligned}$$

leading to

$$\begin{aligned} \chi_{i-1} &= (E_0 - V\chi_i V^T)^{-1} , \\ \bar{\chi}_{i+1} &= (E_0 - V^T\bar{\chi}_i V)^{-1} . \end{aligned} \tag{C14}$$

By means of these recursion relations, it can be shown that χ_i and $\bar{\chi}_i$ are symmetric matrices and are independent of n, as implied in Eq. (C13). Furthermore, because the chain is semi-infinite in one direction, we have $\chi_i = \chi = \text{constant}$; this does not hold true for the $\bar{\chi}_i$. The latter must be calculated individually, starting at the defect and moving down the chain.

In order to calculate the local density of states on each site, we need

$$G_{ii} = \tilde{G}_{ii}S_0 + \tilde{G}_{i,\,i+1}S^T + \tilde{G}_{i,\,i-1}S . \tag{C15}$$

From Eq. (C10),

$$E_0\tilde{G}_{ii} - V\tilde{G}_{i+1,\,i} - V^T\tilde{G}_{i-1,\,i} = 1 ,$$

or

$$\tilde{G}_{ii} = (E_0 - V\chi V^T - V^T\bar{\chi}_i V)^{-1} . \tag{C16}$$

Also,

$$\begin{aligned} \tilde{G}_{i,\,i+1} &= (\tilde{G}_{i+1,\,1})^T = (\chi V^T\tilde{G}_{ii})^T = \tilde{G}_{ii}V\chi , \\ \tilde{G}_{i,\,i-1} &= (\tilde{G}_{i-1,\,i})^T = (\bar{\chi}_i V\tilde{G}_{ii})^T = \tilde{G}_{ii}V^T\bar{\chi}_i , \end{aligned}$$

so that finally Eq. (C15) becomes

$$G_{ii} = \tilde{G}_{ii}(S_0 + V\chi V^T + V^T\bar{\chi}_i S) . \tag{C17}$$

The generalization to the calculation of G_{00} at the defect site itself is straightforward.

[1] H. Fritzsche, in *Amorphous and Liquid Semiconductors*, edited by J. Tauc (Plenum, New York, 1973), p. 221.

[2] J. M. Marshall and E. A. Owen, Philos. Mag. 31, 1341 (1975).

[3] S. C. Agarwal, Phys. Rev. B 7, 685 (1973).

[4] N. F. Mott, E. A. Davis, and R. A. Street, Philos. Mag. 32, 961 (1975).

[5] M. Kastner, J. Non-Cryst. Solids 31, 223 (1978).

[6] S. G. Bishop, U. Strom, and P. C. Taylor, in *The Physics of Selenium and Tellurium*, edited by E. Gerlach and P. Grosse (Springer, New York, 1979), p. 193.

[7] P. W. Anderson, Phys. Rev. Lett. 34, 953 (1975).

[8] R. A. Street and N. F. Mott, Phys. Lett. 35, 1293 (1975).

[9]M. Kastner, D. Adler, and H. Fritzsche, Phys. Rev. Lett. 37, 1504 (1976).
[10]P. W. Anderson, J. Phys. (Paris) 10, suppl. C4 (1976).
[11]D. L. Stein, D. C. Licciardello, and K. B. Ma, Bull. Am. Phys. Soc. 23, 414 (1978).
[12]D. Emin, in *Proceedings of the Eighth International Conference on Liquid and Amorphous Semiconductors, Cambridge, Mass., 1979,* edited by W. Paul and M. Kastner (North-Holland, New York, 1980), p. 969.
[13]R. Kaplow, T. A. Rowe, and B. L. Averbach, Phys. Rev. B 3, 168 (1968).
[14]D. Vanderbilt and J. D. Joannopoulos, Phys. Rev. Lett. 42, 1012 (1979).
[15]J. D. Joannopoulos, in *The Physics of Selenium and Tellurium*, edited by E. Gerlach and P. Grosse (Springer, New York, 1979), p. 2.
[16]B. Moreth, Phys. Rev. Lett. 42, 264 (1979).
[17]D. R. McCann and L. Cartz, J. Appl. Phys. 43, 4473 (1972).
[18]W. Lingelbach, J. Stuke, G. Weiser, and J. Treusch, Phys. Rev. B 5, 243 (1972).
[19]W. B. Pollard and J. D. Joannopoulos, Phys. Rev. B 19, 4217 (1979).
[20]S. G. Bishop, U. Strom, and P. C. Taylor, Phys. Rev. B 15, 2278 (1977).
[21]D. Vanderbilt and J. D. Joannopoulos, Solid State Commun. (in press).
[22]M. A. Abkowitz, in *The Physics of Selenium and Tellurium*, edited by E. Gerlach and P. Grosse (Springer, New York, 1979), p. 210.
[23]J. D. Joannopoulos, Th. Starkloff, and M. Kastner, Phys. Rev. Lett. 38, 660 (1977).
[24]F. Herman and S. Skillman, *Atomic Structure Calculations* (Prentice-Hall, Englewood Cliffs, 1963).
[25]P. Lowdin, J. Chem. Phys. 19, 1396 (1951).
[26]D. J. Chadi and M. L. Cohen, Phys. Rev. B 8, 5747 (1973).
[27]J. C. Slater, *The Self-Consistent Field for Molecules and Solids* (McGraw-Hill, New York, 1974).
[28]D. J. Chadi, Phys. Rev. Lett. 41, 1062 (1978).
[29]D. D. Wagman, W. H. Evans, V. B. Parker, I. Halow, S. M. Bailey, and R. H. Schum, *Selected Values of Chemical Thermodynamic Properties*, U. S. National Bureau of Standards Technical Note 270-3 (U.S. G.P.O., Washington, DC., 1968), p. 56.
[30]K. K. Yee and R. F. Barrow, J. Chem. Soc. Faraday Trans. 2 68, 1181 (1972).
[31]G. Herzberg, *Spectra of Diatomic Molecules* (Van Nostrand, Princeton, 1950), pp. 101–102, 568.
[32]J. D. Joannopoulos and F. Yndurain, Phys. Rev. B 10, 5164 (1974).
[33]J. D. Joannopoulos, Phys. Rev. B 16, 2764 (1977).